OH and HO2 chemistry in clean marine air during SOAPEX-2

R. Sommariva, A.-L. Haggerstone, L. J. Carpenter, N. Carslaw, D. J. Creasey, D. E. Heard, J. D. Lee, A. C. Lewis, M. J. Pilling, J. Zádor

Atmos. Chem. Phys., 4, 839–856, 2004
www.atmos-chem-phys.org/acp/4/839/
SRef-ID: 1680-7324/acp/2004-4-839

Atmospheric Chemistry and Physics

OH and HO_2 chemistry in clean marine air during SOAPEX-2

R. Sommariva[1], A.-L. Haggerstone[2], L. J. Carpenter[2], N. Carslaw[3], D. J. Creasey[1,*], D. E. Heard[1], J. D. Lee[1,], A. C. Lewis[1,**], M. J. Pilling[1], and J. Zádor[4]**

[1]Department of Chemistry, University of Leeds, Leeds, UK
[2]Department of Chemistry, University of York, York, UK
[3]Environment Department, University of York, York, UK
[4]Department of Physical Chemistry, Eötvös University (ELTE), Budapest, Hungary
[*]Now at Photonic Solutions plc., Gracemount Business Pavilions Unit A2/A3, 40 Captains Rd., Edinburgh, UK
[**]Now at Department of Chemistry, University of York, York, UK

Received: 17 December 2003 – Published in Atmos. Chem. Phys. Discuss.: 20 January 2004
Revised: 21 May 2004 – Accepted: 2 June 2004 – Published: 14 June 2004

Abstract. Model-measurement comparisons of HO_x in extremely clean air ([NO]<3 ppt) are reported. Measurements were made during the second Southern Ocean Photochemistry Experiment (SOAPEX-2), held in austral summer 1999 at the Cape Grim Baseline Air Pollution Station in northwestern Tasmania, Australia.

The free-radical chemistry was studied using a zero-dimensional box-model based upon the Master Chemical Mechanism (MCM). Two versions of the model were used, with different levels of chemical complexity, to explore the role of hydrocarbons upon free-radical budgets under very clean conditions. The "detailed" model was constrained to measurements of CO, CH_4 and 17 NMHCs, while the "simple" model contained only the CO and CH_4 oxidation mechanisms, together with inorganic chemistry. The OH and HO_2 (HO_x) concentrations predicted by the two models agreed to within 5–10%.

The model results were compared with the HO_x concentrations measured by the FAGE (Fluorescence Assay by Gas Expansion) technique during four days of clean Southern Ocean marine boundary layer (MBL) air. The models overestimated OH concentrations by about 10% on two days and about 20% on the other two days. HO_2 concentrations were measured during two of these days and the models overestimated the measured concentrations by about 40%. Better agreement with measured HO_2 was observed by using data from several MBL aerosol measurements to estimate the aerosol surface area and by increasing the HO_2 uptake coefficient to unity. This reduced the modelled HO_2 overestimate by ∼40%, with little effect on OH, because of the poor HO_2 to OH conversion at the low ambient NO_x concentrations.

Local sensitivity analysis and Morris One-At-A-Time analysis were performed on the "simple" model, and showed the importance of reliable measurements of $j(O^1D)$ and [HCHO] and of the kinetic parameters that determine the efficiency of $O(^1D)$ to OH and HCHO to HO_2 conversion. A 2σ standard deviation of 30–40% for OH and 25–30% for HO_2 was estimated for the model calculations using a Monte Carlo technique coupled with Latin Hypercube Sampling (LHS).

Correspondence to: M. J. Pilling
(m.j.pilling@chemistry.leeds.ac.uk)

1 Introduction

Tropospheric chemistry is strongly dependent on the concentration of the hydroxyl radical (OH), which reacts very quickly with most trace gases in the atmosphere. Owing to its short boundary layer lifetime (∼1 s), atmospheric concentrations of OH are highly variable and respond rapidly to changes in concentrations of sources and sinks. Photolysis of ozone, followed by reaction of the resulting excited state oxygen atom with water vapour, is the primary source of the OH radical in the clean troposphere:

$$O_3 + h\nu\ (\lambda < 340\ \text{nm}) \rightarrow O(^1D) + O_2 \quad (1)$$

$$O(^1D) + H_2O \rightarrow OH + OH \quad (2)$$

About 10% of the $O(^1D)$ atoms react through Reaction (2) under typical boundary layer conditions, the rest are deactivated to the ground state through collisions with N_2 and O_2, reforming ozone.

The two major tropospheric sinks of OH are the reactions with CO and CH_4. In the clean Southern Hemisphere, CO and CH_4 account for up to 50% each of the total OH loss, and HO_2 and CH_3O_2 are the predominant forms of peroxy radicals formed (Reactions 3, 4, respectively).

$$CO + OH + O_2 \rightarrow CO_2 + HO_2 \quad (3)$$

$$CH_4 + OH + O_2 \rightarrow CH_3O_2 + H_2O \quad (4)$$

The OH radical also reacts with non methane hydrocarbons (NMHCs) producing a variety of organic peroxy radicals (RO_2). HO_2 and CH_3O_2 react with NO producing OH and CH_3O, respectively (Reactions 5, 6).

$$HO_2 + NO \rightarrow OH + NO_2 \quad (5)$$

$$CH_3O_2 + NO \rightarrow CH_3O + NO_2 \quad (6)$$

However in low NO_x conditions peroxy radicals primarily react through self and cross peroxy-peroxy reactions to form methyl hydrogen peroxide (CH_3OOH) and hydrogen peroxide (H_2O_2). HO_2 is also recycled back to OH through the reaction with O_3 (Reaction 9).

The self reaction of CH_3O_2 also gives CH_3O (Reaction 10) with a branching ratio of 0.33, other pathways leading to the formation of CH_3OH and HCHO. The reaction of CH_3O with O_2 (Reaction 11) is one of the main sources of HCHO and a very important source of HO_2.

$$HO_2 + HO_2 \rightarrow H_2O_2 + O_2 \quad (7)$$

$$CH_3O_2 + HO_2 \rightarrow CH_3OOH + O_2 \quad (8)$$

$$HO_2 + O_3 \rightarrow OH + 2O_2 \quad (9)$$

$$CH_3O_2 + CH_3O_2 \rightarrow 2CH_3O + O_2 \quad (10)$$

$$CH_3O + O_2 \rightarrow HCHO + HO_2 \quad (11)$$

The methyl hydrogen peroxide contributes to OH loss via Reactions (12) and (13) to form CH_3O_2 and HCHO.

$$CH_3OOH + OH \rightarrow CH_3O_2 \quad (12)$$

$$CH_3OOH + OH \rightarrow HCHO + OH \quad (13)$$

In studies comparing measured and modelled HO_x radical concentrations, the models usually overestimate [OH] by 20–50%. A detailed review of the comparisons of modelled and measured concentrations of OH and HO_2 can be found in Heard and Pilling (2003). In particular, several studies have been made in the marine boundary layer.

Eisele et al. (1996) showed that modelled [OH] overestimated measurements by a factor of 2 during the MLOPEX-2 campaign. During EASE96 modelled [OH] results were higher than the measurements by ∼40% (Carslaw et al., 1999), while in EASE 97 the model-measurement ratio was on average 2.1 in clean air conditions (Carslaw et al., 2002). During the ALBATROSS campaign, in the Southern Atlantic, Brauers et al. (2001) overestimated OH by 16% on average, while during the WAOSE95 campaign, the agreement between the model and the measurements was ∼50% or better (Grenfell et al., 1999). In three recent aircraft campaigns in the Pacific Ocean, PEM Tropics A and B and ACE-1, the agreement between modelled and measured OH was 15–20% in PEM Tropics A and ∼30% in ACE-1 (Chen et al., 2001; Frost et al., 1999) while in PEM Tropics B the model to observed ratio was 1.22 on average at the surface (Tan et al., 2001).

There have been fewer measurements of HO_2 in the MBL. The agreement between modelled and measured [HO_2] is variable. Some studies show a reasonable agreement with the measurements (within 25%), but generally the models tend to overestimate [HO_2] by a factor of 2 or more (Carslaw et al., 1999, 2002; Kanaya et al., 2000, 2001). In PEM Tropics B Tan et al. (2001) reported a modelled to observed ratio of 1.12 for HO_2 near the surface.

This paper investigates the radical chemistry of the clean marine boundary layer in the Southern Ocean during the SOAPEX-2 (Southern Ocean Photochemistry Experiment 2) campaign using an observationally constrained box-model based on the Master Chemical Mechanism (Jenkin et al., 1997, 2003; Saunders et al., 2003). The primary aim of SOAPEX-2 was to study free radical chemistry in the remote marine boundary layer in the Southern Hemisphere. Sections 2 and 3 of this paper describe the SOAPEX-2 site and the measurements that were made during the campaign. Section 4 describes the models used and Sect. 5 presents the results. Finally, Sect. 6 contains the summary and the conclusions.

2 Site description

The SOAPEX-2 campaign, involving scientists from the Universities of East Anglia, Leeds and Leicester, from the CSIRO (Commonwealth Scientific and Industrial Research Organization) Melbourne and from the Australian Bureau of Meteorology, took place in austral summer during the period 18 January to 18 February 1999 at the Cape Grim Baseline Atmospheric Pollution Station (CGBAPS). The station is situated on the north-west tip of Tasmania, Australia, at 40°41′ S, 144°41′ E, on a cliff-top ∼100 m above sea level and ∼100 m horizontally from the high-water mark. CGBAPS is part of the World Meteorological Organisation network of Global Atmospheric Watch observatories and an extensive program of atmospheric chemistry and meteorological measurements has been carried out at the site since 1976. Further details about the site are given in Bates et al. (1998).

Cape Grim is an ideal location to study free-radical chemistry in extremely clean conditions (Penkett et al., 1997). It frequently experiences air masses characterized by low condensation nuclei (CN) and Radon counts ($<462\,cm^{-3}$ and $<100\,mBq\,m^{-3}$, respectively) with the local wind direction in the sector 190°–280°. In these "baseline" conditions, air has not passed over land for 5 days or more and is therefore relatively free of anthropogenic influence. Four days, which were characterised by the lowest NO_x and NMHCs levels experienced during the campaign, have been selected to be representative of baseline conditions in the Southern Ocean.

Table 1. Measurements and techniques during SOAPEX-2.

Measurement	Technique	Average Uncertainty	Institution
OH	FAGE [a]	40%	University of Leeds
HO_2	FAGE [a]	50%	University of Leeds
NMHCs (C_2-C_7)	GC-FID [b]	7%	University of Leeds
CH_4	GC-FID [c,h,i]	0.1%	CGBAPS/AGAGE
CO	GC-HgO[c,i]	1%	CGBAPS/AGAGE
$j(O^1D)$	2π filter radiometer [a,d]	25%	Universities of Leeds and Leicester
$j(NO_2)$	2π and 4π filter radiometer [d]	5%	University of Leicester
NO	4 channel chemiluminiscence [e]	10%	University of East Anglia
NO_2	4 channel chemiluminiscence [e]	28%	University of East Anglia
HCHO	Fluorimetry [f]	50%	CGBAPS
O_3	UV absorption spectroscopy [a,c]	3–5%	CGBAPS and University of Leeds
H_2O_2, CH_3OOH	HPLC fluorometric [d]	10%	CGBAPS
HO_2+ΣRO_2	PERCA [d]	30%	University of Leicester
NO_3	DOAS [g]	25%	University of East Anglia
IO	DOAS [g]	20%	University of East Anglia
OIO	DOAS [g]	30%	University of East Anglia
PAN	GC-ECD	26%	University of East Anglia
H_2O	IR absorption spectroscopy [a,c]	1–2%	CGBAPS and University of Leeds
Temperature, wind speed and direction	Meteorological station [a,c]	0.5%	CGBAPS and University of Leeds

[a] Creasey et al. (2002, 2003).
[b] Lewis et al. (2001).
[c] Bureau of Meteorology and CSIRO Division of Atmospheric Research, Baseline Atmospheric Program reports, Melbourne, Australia, 1976–1995.
[d] Monks et al. (1998).
[e] Bauguitte (1998, 2000).
[f] Ayers et al. (1997).
[g] Allan et al. (2001).
[h] Cunnold et al. (2002).
[i] Prinn et al. (2000).

3 Experimental

During SOAPEX-2, measurements of the free-radicals OH, HO_2, HO_2+ΣRO_2, NO_3, IO and OIO were supported by measurements of temperature, wind speed and direction, photolysis rates ($j(O^1D)$ and $j(NO_2)$), water vapor, O_3, HCHO, CO, CH_4, NO, NO_2, peroxyacetyl nitrate (PAN), a wide range of NMHCs, organic halogens, H_2O_2, CH_3OOH and condensation nuclei (CN).

Concentrations of OH and HO_2 were determined, in situ, using Laser Induced Fluorescence (LIF) at low pressure, (FAGE technique). HO_2 cannot be detected directly by LIF, and was converted to OH by titration with NO directly below the sampling nozzle. The detection limit for the FAGE instrument during SOAPEX-2, determined by calibration in the field, was 1.4×10^5 molecule cm^{-3} for OH and 5.4×10^5 molecule cm^{-3} for HO_2. A description of the instrument, as set up in previous field campaigns and during SOAPEX-2, along with the calibration procedure, is provided elsewhere (Creasey et al., 2002, 2003).

Light non-methane hydrocarbons (NMHCs) were measured using an automated GC-FID system with large volume sample collection onto a Peltier cooled carbon sieve trap followed by on-line thermal desorption, and separation on an aluminium oxide PLOT capillary column. The system deployed at Cape Grim has been described in more detail in a previous paper (Lewis et al., 2001).

The techniques used to measure the other species and parameters are listed in Table 1.

4 Model description

Two versions of a zero-dimensional box-model, containing different chemical schemes, were used to investigate the atmospheric chemistry of the SOAPEX-2 campaign. Both the

Table 2. Average percentage OH loss due to CO, CH_4 and NMHCs during four clean days in SOAPEX-2 (Note that the figures have been rounded up or down to the nearest 0.1%).

	7 Feb.	8 Feb.	15 Feb.	16 Feb.
CO	46.4	43.2	50.6	46.7
CH_4	48.4	44.0	44.5	49.3
ethane	0.2	0.1	0.2	0.2
ethene	0.3	0.4	0.2	0.2
propane	0.0	0.0	0.2	0.1
propene	0.5	0.7	0.4	0.5
acetylene	0.0	0.0	0.1	0.0
i-butane	0.0	0.0	0.1	0.1
t-2-butene	0.0	1.8	0.0	0.0
1-butene	0.2	0.6	0.1	0.0
c-2-butene	0.0	1.9	0.0	0.0
n-pentane	0.1	0.1	0.1	0.1
t-2-pentene	0.0	1.3	0.0	0.0
c-2-pentene	0.0	1.1	1.1	0.0
isoprene	1.1	2.4	1.1	1.1
DMS	2.4	2.0	1.0	1.6
benzene	0.1	0.1	0.1	0.1
toluene	0.1	0.1	0.2	0.1
DMDS	0.2	0.1	0.2	0.1
Total	100.0	99.9	100.2	100.2

"simple" and the "detailed" models were constrained with the observed concentrations of the longer lived species: NO_x, O_3, CO, CH_4, and HCHO as well as the values of $j(O^1D)$, $j(NO_2)$, H_2O and temperature. A boundary layer height of 1 km was assumed (Ayers and Galbally, 1994). The "detailed" model also contained a full chemical scheme for 17 of the measured NMHCs (see Sect. 4.1). The models were then employed to calculate in situ OH and HO_2 concentrations, for comparison with each other and the results from the FAGE instrument.

4.1 The "detailed" model

The "detailed" model was constructed as described by Carslaw et al. (1999, 2002). Briefly, measurements of NMHCs, CO and CH_4 were used to define a reactivity index with OH, in order to determine which NMHCs, along with CO and CH_4, to include in the overall mechanism. The product of the concentration of each hydrocarbon (and CO) measured on each day during the campaign and its rate coefficient for the reaction with OH was calculated. All NMHCs that are responsible for at least 0.1% of the OH loss due to total hydrocarbons and CO on any day during the campaign are included in the mechanism (Table 2). Reactions of OH with the secondary species formed in the hydrocarbon oxidation processes, as well as oxidation by the nitrate radical (NO_3) and ozone are also included in the mechanism. The NMHCs that were found to be important for the SOAPEX-2 campaign were ethane, propane, isobutane, n-pentane, ethene, propene, trans-2-butene, cis-2-butene, 1-butene, trans-2-pentene, cis-2-pentene, acetylene, isoprene, DMS (dimethylsulphide), benzene, toluene and DMDS (dimethyldisulphide). In clean conditions, these 17 NMHCs contributed on average about 5% to the OH loss, while CO and CH_4 accounted for about 95% (with the exception of 8 February on which NMHCs accounted for almost 13% of OH loss). The relative contributions of CO, CH_4, DMS, DMDS and NMHCs to OH loss during the four modelled days are shown in Table 2.

The mechanisms for the NMHCs (except DMS) required to fully characterise OH chemistry were extracted from a recently updated version of the Master Chemical Mechanism (MCM 3.0, available at http://mcm.leeds.ac.uk/MCM/). The MCM treats the degradation of 125 volatile organic compounds (VOCs) and considers oxidation by OH, NO_3, and O_3, as well as the chemistry of the subsequent oxidation products. These steps continue until CO_2 and H_2O are formed as final products of the oxidation. The MCM has been constructed using chemical kinetics data (rate coefficients, branching ratios, reaction products, absorption cross sections and quantum yields) taken from several recent evaluations and reviews or estimated according to the MCM protocol (Jenkin et al., 1997, 2003; Saunders et al., 2003). The MCM is an explicit mechanism and, as such, does not suffer from the limitations of a lumped scheme or one containing surrogate species to represent the chemistry of many species.

The DMS scheme has been taken from the work of Koga and Tanaka (1993), with many of the rate coefficients updated as suggested by Jenkin et al. (1996). The reactions of NO_3, from the Yin et al. (1990a, b) mechanism, have also been included.

DMDS was detected at a maximum concentration for clean conditions of 0.38 ppt during SOAPEX-2. The degradation of DMDS by both OH and NO_3 has been included according to Jenkin et al. (1996), as well as its photolysis to form two CH_3S molecules (Yin et al., 1990a, b). The oxidation products are common to DMS.

Previous work has suggested that Cl atoms may have a bearing on the concentration of many hydrocarbon species, particularly in the marine boundary layer (Keene et al., 1996; Pszenny et al., 1993). The degradation of chlorinated organic species leads ultimately to the release of Cl atoms. Although Cl reacts with O_3, it also reacts rapidly with many organic compounds. Following the protocol for the MCM laid down by Jenkin et al. (1997), we assume that Cl is removed only by reactions with alkanes, as these are less reactive towards OH and are generally present at higher concentrations than other organic species. The precursor species included in the mechanism are $CHCl_3$, CH_2Cl_2, CH_3Cl and C_2Cl_4, the concentrations of which were all determined in this campaign, albeit at low frequency.

The "detailed" model contains 2085 gas-phase reactions, 19 heterogeneous and 116 deposition processes.

4.2 The "simple" model

The "simple" model contained the same inorganic and CO-CH_4 oxidation schemes as the "detailed" model, taken from the MCMv3. The model was completed with heterogeneous loss and dry deposition terms, as described in the following section. The chemical mechanism employed in the "simple" model contains 75 gas-phase reactions, 9 heterogeneous and 8 deposition processes and is shown in Table 7.

4.3 Heterogeneous uptake and dry deposition

The models consider a simple parameterization for heterogeneous loss, where it is assumed that radicals are irreversibly lost upon impacting on aerosol, according to:

$$k_{het} = \frac{A\bar{c}\gamma}{4} \quad (14)$$

where γ is the gas/surface reaction probability, A is the reactive aerosol surface area per unit volume (RASA) (cm^{-1}) and $\bar{c}$ is the mean molecular speed ($cm\,s^{-1}$) (Ravishankara, 1997). There are several species formed in the DMS mechanism – DMSO, $DMSO_2$ (dimethylsulphone, $CH_3S(O_2)CH_3$) and MSA (methane sulfinic acid, $CH_3S(O)OH$) – that are likely to be readily condensed on existing particles due to their strong hygroscopic nature and low vapour pressure (Koga and Tanaka, 1993).

Heterogeneous uptake on surfaces has also been documented for various free radicals (DeMore et al., 1994). Table 3 shows values of the gas/surface reaction probabilities (γ) of the species assumed to undergo loss to aerosol surface in the model. Only the species where a reaction probability has been measured at a reasonable boundary layer temperature (i.e. >273 K) and on a suitable surface for the marine boundary layer ($NaCl_{(s)}$ or liquid water) have been included. Unless stated otherwise, values for uptake onto $NaCl_{(s)}$, the most likely aerosol surface in the MBL (Gras and Ayers, 1983), have been used. Where reaction probabilities are unavailable mass accommodation coefficients (α) have been used instead. The experimental values of the reaction probability are expected to be smaller than or equal to the mass accommodation coefficients because α is just the probability that a molecule is taken up on the particle surface, while γ takes into account the uptake, the gas phase diffusion and the reaction with other species in the particle (Ravishankara, 1997).

Large uncertainties exist in the values of these reaction probability coefficients, which tend to vary greatly with both temperature and type of surface.

Dry deposition terms have also been incorporated in the model based on the values of Derwent et al. (1996) except for peroxides (1.1 $cm\,s^{-1}$ for H_2O_2 and 0.55 $cm\,s^{-1}$ for organic peroxides), methyl and ethyl nitrate (1.1 $cm\,s^{-1}$) and HCHO (0.33 $cm\,s^{-1}$) (Brasseur et al., 1998) and it has been assumed that the dry deposition velocity for CH_3CHO and other aldehydes is the same as that for HCHO.

Table 3. Reaction probabilities for the heterogeneous loss processes used in the model.

Species	γ	Reference
OH	$1.25\times10^{-5}e^{(1750/T)}$ (a)	Gratpanche et al. (1996)
HO_2	$1.40\times10^{-8}e^{(3780/T)}$ (a)	Gratpanche et al. (1996)
CH_3O_2	4×10^{-3} (at 296 K)	Gershenzon et al. (1995)
NO_3	4×10^{-3} (at 282–286 K) (b)	Allan et al. (1999)
N_2O_5	0.032 (at 291 K)	Behnke et al. (1997)
HNO_3	0.014 (at 298 K)	Beichert and Pitts (1996)
MSA	0.11 (at 278 K) (c,d)	DeBruyn et al. (1994)
SO_2	0.11 (at 260–292 K) (c,d)	Worsnop et al. (1989)
DMSO	0.08 (at 281 K) (c,d)	DeBruyn et al. (1994)
$DMSO_2$	0.08 (at 281 K) (c,d)	DeBruyn et al. (1994)
H_2O_2	0.1 (at 292 K) (c,d)	Worsnop et al. (1989)
CH_3OH	0.02 (at 291 K) (c,d)	Jayne et al. (1991)
C_2H_5OH	0.02 (at 291 K) (c,d)	Jayne et al. (1991)
1-propanol	0.02 (at 291 K) (c,d)	Jayne et al. (1991)
2-propanol	0.02 (at 291 K) (c,d)	Jayne et al. (1991)
$HOCH_2CH_2OH$	0.04 (at 291 K) (c,d)	Jayne et al. (1991)
$CH_3C(O)CH_3$	0.013 (at 285 K) (c,d)	Duan et al. (1993)
HC(O)OH	0.02 (at 291 K) (c,d)	Jayne et al. (1991)
$CH_3C(O)OH$	0.03 (at 291 K) (c,d)	Jayne et al. (1991)

(a) value at relevant temperature.
(b) estimated by using average of results of Rudich et al. (1996).
(c) measured on liquid water aerosols.
(d) mass accommodation coefficient.

4.4 Effect of new recommendations for rate coefficients

Although the MCMv3.0 was completed quite recently, there have already been some new recommendations for several of the inorganic rate coefficients, which have been incorporated into both the simple and detailed models. The largest changes concern the pressure-dependent reactions of OH with CO and NO_2. The rate coefficient of OH and CO has decreased by 16% (from 2.43×10^{-13} to 2.05×10^{-13} cm^{-3} $molecule^{-1}$ s^{-1} at 298 K), while that of OH and NO_2 has increased by 35% (from 8.95×10^{-12} to 1.21×10^{-11} cm^{-3} $molecule^{-1}$ s^{-1} at 298 K) under typical boundary layer conditions (Atkinson et al., 2001). Rate coefficients for the reactions of HO_2 with HO_2 and O_3 have also been revised following recent laboratory measurements. The difference in [OH] and [HO_2] before and after updating these rate coefficients is small: less than a 10% increase for OH and less than a 2% increase for HO_2.

In MCMv3.0 the quenching reaction of $O(^1D)$ with N_2 has a rate coefficient of 2.58×10^{-11} cm^{-3} $molecule^{-1}$ s^{-1} at 298 K (Atkinson et al., 2001). Recently three groups reported a new rate coefficient of 3.09×10^{-11} cm^{-3} $molecule^{-1}$ s^{-1}

Table 4. Average (11:00–14:00) measurements during the clean days.

Measurements	7 Feb.	8 Feb.	15 Feb.	16 Feb.
H_2O/molecule cm^{-3}	2.5×10^{17}	3.3×10^{17}	3.4×10^{17}	3.7×10^{17}
$j(O^1D)/s^{-1}$	2.2×10^{-5}	2.9×10^{-5}	3.5×10^{-5}	2.8×10^{-5}
$j(NO_2)/s^{-1}$	8.9×10^{-3}	9.1×10^{-3}	9.7×10^{-3}	8.3×10^{-3}
O_3/ppb	14.9	13.5	18.5	17.6
NO/ppt	0.8	3.7	1.5	2.4
NO_2/ppt	7.5	8.8	12.1	14.8
CH_4/ppb	1687	1694	1685	1686
CO/ppb	40.7	45.6	39.9	39.6
HCHO/ppt	352	217	322	244
Temperature/°C	14.5	16.2	18.6	17.1

Table 5. Average (11:00–14:00) and maximum measured [OH] and [HO_2] in molecule cm^{-3}.

Measurements	7 Feb.	8 Feb.	15 Feb.	16 Feb.
OH				
Average	1.9×10^6	2.3×10^6	2.7×10^6	2.5×10^6
Maximum	2.6×10^6	3.1×10^6	3.5×10^6	3.6×10^6
HO_2				
Average	–	–	1.7×10^8	1.4×10^8
Maximum	–	–	1.9×10^8	2.1×10^8

at 298 K (Ravishankara et al., 2002). The effect of the new rate coefficient is to decrease the OH concentration by ∼10% and HO_2 by ∼2% for SOAPEX-2 clean conditions.

The effect of using a new rate coefficient for the reaction HO_2+NO of 8.41×10^{-12} cm^{-3} molecule^{-1} s^{-1} at 298 K (C. Percival, personal communication) instead of the 8.91×10^{-12} cm^{-3} molecule^{-1} s^{-1} at 298 K used in the MCMv3.0 (Atkinson et al., 2001) was negligible for both HO_2 and OH for the clean conditions studied: for example, the variation in [HO_2] is about 0.02% at midday on 7 February.

The cumulative effect of updating the model and using the new rate coefficient for the reaction $O(^1D)+N_2$ is negligible (<2%).

5 Results and discussion

Airflows reaching the site were characterised according to air mass origin, determined from windfield back trajectories calculated using the European Centre for Medium Range Weather Forecasts (ECMWF) trajectory package, supplied by the British Atmospheric Data Centre (http://www.badc.nerc.ac.uk/community/trajectory/). The average concentrations of the most important species and parameters measured during the clean days (7, 8, 15, and 16 February) are shown in Table 4.

The concentrations of nitrogen oxides measured on the clean days were very low. Typical daytime concentrations were around 3 ppt of NO and 10 ppt of NO_2 on 7 and 8 February and around 2 ppt of NO and 15 ppt of NO_2 on 15 and 16 February (Table 4).

The complete datasets of OH and HO_2 measurements during SOAPEX-2 are described in detail in Creasey et al. (2003).

5.1 OH measured to modelled comparisons

Daily measurements of OH by FAGE began between 07:00 and 10:00 and finished at about 18:00. On 15 February the measurements continued until 23:00 and were started on 16 February at 05:40. The late evening and early morning measurements show a concentration of OH of the order of 1×10^5 molecule cm^{-3}. The average and maximum measured [OH] are shown in Table 5.

Figures 1 and 2 show the modelled and measured OH concentrations. The agreement is quite good around midday (10:00–14:00): the models overestimate [OH] by <10% on 7–8 February and <30% on 15–16 February. It should be noted that the concentration of NO is slightly higher on 15 and 16 February (up to 5 ppt) than on 7 and 8 February (up to 3 ppt).

The models reproduce the OH structure, which is due to the passage of clouds, quite well. During these days $j(O^1D)$ tracks OH closely; Creasey et al. (2003) reported a high correlation (r=0.95) between measured [OH] and the rate of OH production from ozone photolysis during clean days in SOAPEX-2. There is a tendency for the model profiles to overestimate [OH] before and after this midday period (see especially 8 and 16 February). As discussed in Sect. 5.3, the feedback from HO_2 to OH, via reaction with O_3 and NO, is significantly less than formation of OH via ozone photolysis, so that a neglected sink is the most likely explanation of this discrepancy, although its identity is not clear. On day 15, there is a significant evening "tail" in the OH concentration, that the model does not reproduce. The "tail" will be discussed further in Sect. 5.2.

Figures 3 and 4 show the scatter plots for the "detailed" model for the four clean days, together with a 1:1 line representing the case of an ideal agreement. The model clearly has a tendency to overestimate the measured [OH]. In particular on 15 and 16 February the scatter plots are well below the 1:1 line, except for low values of OH, which correspond to the evening "tail". The scatter plots for 15 and 16 February also have the same slope indicating the similarity between the two days. 7 February shows the best agreement between the model and the measurements.

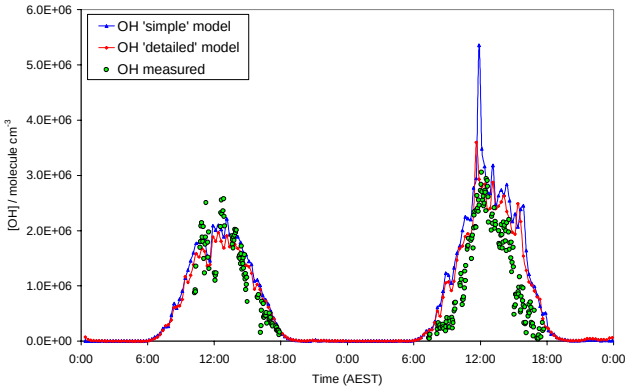

Fig. 1. Model-measurement comparison of OH (7–8 February).

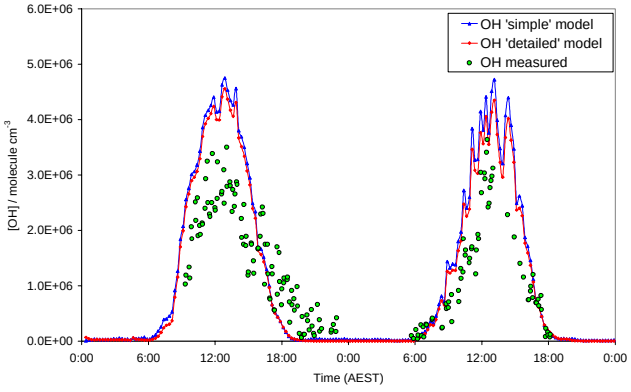

Fig. 2. Model-measurement comparison of OH (15–16 February).

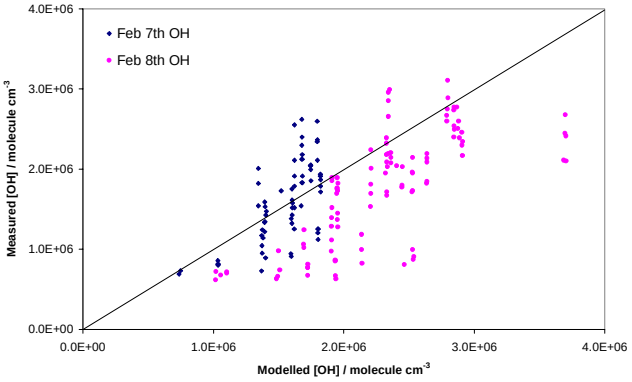

Fig. 3. Modelled-measured OH scatter plots.

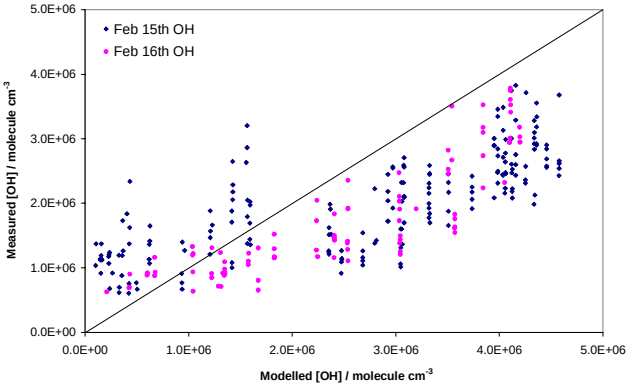

Fig. 4. Modelled-measured OH scatter plots.

5.2 HO_2 measured to modelled comparisons

HO_2 measurements during SOAPEX-2 were available only from 9 February onwards due to technical difficulties and so the comparison is possible only for 15 and 16 February, under clean conditions. On 15 February measurements were from 09:25 until 23:00, on 16 February from 05:40 until 18:15. The late evening and early morning measurements show a concentration of HO_2 of about 2×10^7 molecule cm^{-3}. The average and maximum measured [HO_2] are shown in Table 5. The agreement between the models and the measurements is roughly within a factor of 2 around midday, which is better than was found in previous modelling results for HO_2 (Carslaw et al., 1999, 2001; George et al., 1999; Kanaya et al., 2000; Stevens et al., 1997).

The agreement between the "simple" and the "detailed" models is also very good (within 5% on all the modelled days). The models calculate a night time HO_2 concentration of about 1×10^7 molecule cm^{-3}: however the late evening and early morning measurements are nearly twice this value (Fig. 5), suggesting that the models consistently underestimate the night time concentrations. The night time chemistry will be further discussed in Sect. 5.3.

The scatter plots of modelled vs. measured [HO_2] for the "detailed" model on 15 and 16 February are shown in Fig. 6. While on 16 February the model/measurements ratio appears to be roughly constant throughout the day, on 15 February the model overestimation appears to be higher at high [HO_2] and gets closer to a 1:1 ratio at low [HO_2].

As with OH, there is a tendency to overestimate the concentrations by a larger factor before and after the midday period, except for the "tail" on the evening of 15 February. The "HO_2 tail" is analogous to the one observed in the same period (17:30–23:00) for OH and is clearly visible in the scatter plot (Fig. 6). As will be shown in Sect. 5.3 the recycling between OH and HO_2 is rather slow, owing to the low concentration of NO. Since the "tail" is present for both radicals, and since the rate of conversion of OH to HO_2 is much faster than that from HO_2 to OH, the most likely origin of the tail is a neglected source of OH, but no experimental evidence for its origin is available.

The measured [OH]/j(O^1D) ratio shows a sudden increase of more than an order of magnitude after 18:00 on 15 February, supporting the proposal of an additional OH source. A possibility is the reaction of ozone with biogenic alkenes, but this would require an unrealistic concentration

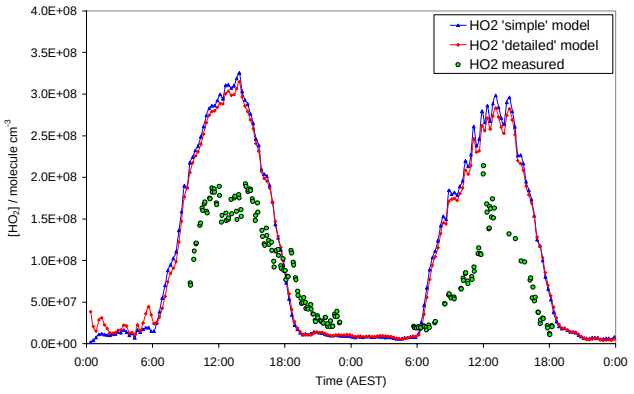

Fig. 5. Model-measurement comparison of HO_2 (15–16 February).

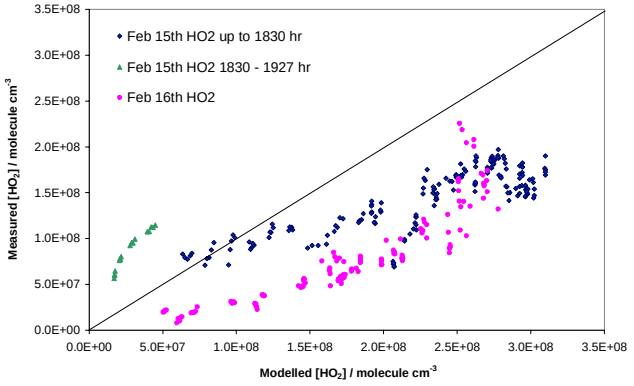

Fig. 6. Model-measurement HO_2 scatter plots.

of monoterpenes (of the order of ppm). Though this cannot be completely ruled out, the cause of the "evening tail" of 15 February remains unknown.

5.3 Rates of production and destruction of HO_x

Calculation of the rates of radical production and loss facilitates an understanding of the key components of the chemical mechanism driving the oxidation chemistry. Figure 7 shows a reaction rate diagram for noon on 7 February. The small imbalances between the rates of production and loss for a given radical reflect the neglect of minor reactions. The relative rates of reactions shown in Fig. 7 are approximately maintained on all four of the days modelled and throughout the daylight hours (06:00–19:00) on those days.

The major source of free-radicals is via $O(^1D)+H_2O$, although there is a substantial route to HO_2 via HCHO photolysis. This observation is based on the measured concentrations of HCHO, which cannot be accounted for by methane chemistry under the conditions pertaining. Ayers et al. (1997) suggested that isoprene might act as a source, but this cannot explain [HCHO] on 7 February, because the measured isoprene concentrations were low ($\leq$2 ppt). The

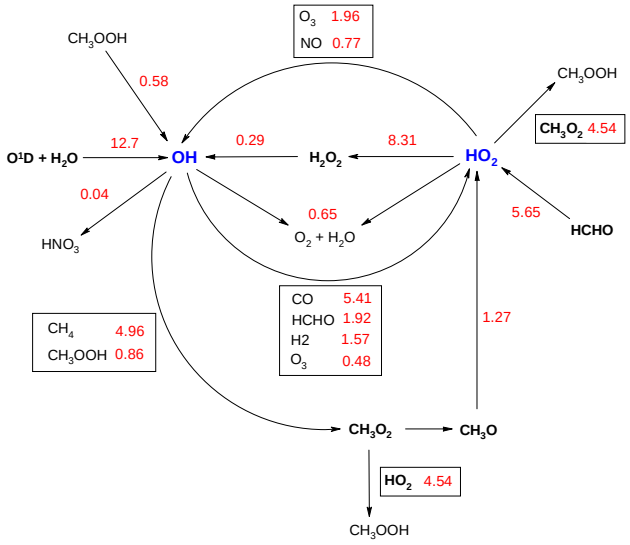

Fig. 7. Fluxes of free-radicals at 12:00 on 7 February, in units of 10^5 molecule cm^{-3} s^{-1}.

source of HCHO on 7 February is not evident, but it clearly plays an important role in radical initiation.

Termination occurs almost exclusively via peroxy-peroxy reactions (HO_2+HO_2 and CH_3O_2+HO_2), with very little formation of HNO_3, but with a small contribution from OH+HO_2. The peroxides (H_2O_2 and CH_3OOH) act as minor sources of OH, slightly reducing the effectiveness of the quadratic terminations.

Propagation from OH occurs mainly via CH_4 and CO. The low [NO] drastically reduces the effectiveness of further propagation from CH_3O_2 and HO_2, with propagation/termination ratios of 0.22 and 0.17, respectively. Formation of OH from HO_2, which completes the propagation cycle, occurs principally by reaction with O_3, rather than NO, and the net chain reaction is a sink for ozone. It is difficult to define a simple chain length for the system, because there are two initiation points in the chain cycle. However, defining an approximate chain length as the ratio of the rate of formation of OH via propagation to the total rate of initiation gives a value of only 0.14, emphasising the inefficiency of the chain cycle under these low NO_x conditions. The analysis also confirms the strong correlation between [OH] and $j(O^1D)$ (r=0.95), noted by Creasey et al. (2003). While HCHO is a significant radical source, the fraction of HO_2 so generated that forms OH is small and OH formation is dominated (78% of the total) by O^1D+H_2O.

There are close parallels between this analysis and that made for the PEM Tropics A campaign (Chen et al., 2001). The percentage contributions of the main OH formation reactions were $O(^1D)+H_2O$=81% (78%), HO_2+O_3=5% (12%), HO_2+NO=4% (5%) and $CH_3OOH+h\nu$=2% (4%) the SOAPEX-2 results shown in brackets. H_2O_2 photolysis contributed 8% of the total in PEM Tropics A, but only 2% in

SOAPEX-2. The dominant OH sinks were CO=34% (34%), CH_4=27% (31%) and CH_3OOH=11% (5%).

It should also be noted that Chen et al. (2001) used a model with a vertical transport component and they do not specify which height the fluxes they report refer to.

The major difference in the two sets of results relates to the significance of HCHO as a radical source. HCHO was not measured in the P-3B flight in PEM Tropics A and is not quoted as a significant HO_x source, while it contributes 30% of the total rate of initiation in SOAPEX-2. This discrepancy emphasizes the importance of a better understanding the HCHO budget. HCHO was measured during the PEM Tropics B campaign. While it was a HO_x source at higher altitudes, for altitudes lower than 1 km it accounted for <5%.

Modelled [HO_2] is non-zero during the night of 15–16 February (Fig. 5) and shows a slow decay over several hours. HO_x and RO_x production is negligible under these clean conditions, but the chain cycle continues with OH reacting with CO and HO_2 with O_3. The relative pseudo-first order rate constants of these reactions, and of OH with CH_4, ensure that [HO_2]≫[OH], with [HO_2]/[OH] larger than during the day. Termination occurs via peroxy-peroxy reactions, but is very slow under the night time low radical concentrations, accounting for the long lifetime of the radical pool, which is dominated by HO_2. Monks et al. (1996) suggested that night time [CH_3O_2] was much greater than [HO_2] at Cape Grim during the SOAPEX-1 campaign, so that CH_3O_2+CH_3O_2 and CH_3O_2+HO_2 dominated termination. They assumed [NO_x]=1 ppt. Measurements of [NO] in SOAPEX-2 showed [NO]<8 ppt during the night of 15–16 February. Under these conditions, the lifetime of CH_3O_2 at night, and as [CH_3O_2] falls, becomes determined by CH_3O_2+NO and propagation from CH_3O_2 to HO_2 via CH_3O becomes efficient.

5.4 Treatment of aerosol loss in the model

There is substantial uncertainty about the effect of aerosol uptake on OH and HO_2 concentrations, mainly due to a lack of ancillary aerosol data recorded during many of the recent MBL campaigns (Carslaw et al., 1999; Kanaya et al., 2000, 2001).

Aerosol surface area is likely to be variable even within a remote marine air mass. Previous MBL aerosol studies describe changes in aerosol concentration and composition due to entrainment from the free troposphere (Bates et al., 1998, 2001; Covert et al., 1998). Raes et al. (1997) found an observable link between vertical transport patterns and aerosol variability in the MBL specifically in the Aitken mode ($<0.2\,\mu$m). Hence entrainment of aerosol from the free troposphere appears to occur frequently, even in remote MBL air masses. In addition, aerosols have the capacity to travel great distances in the free troposphere, before being entrained into the MBL.

Reactive aerosol surface area (RASA) data were not available for SOAPEX-2 so a constant value of $1.0\times10^{-7}\,cm^{-1}$, representative of clean marine boundary layer conditions was used in the standard model runs described thus far (Whitby and Sverdrup, 1980). In addition, a range of appropriate MBL RASA values were calculated from literature data (Bates et al., 1998, 2001; Covert et al., 1998; Raes et al., 1997). RASA can be approximated as the total surface area of aerosols, A_{tot}, easily calculated from the mode fit parameters of lognormal number distributions, R_N (the median droplet radius), N_{tot} (the total number density of aerosol particles), and σ (the deviation from the median in a lognormal distribution) (Sander, 1999):

$$A_{tot} = 4\pi R_N^2 N_{tot} e^{\frac{2(\lg\sigma)^2}{(\lg e)^2}} \quad (15)$$

The mode fit parameters were used to calculate RASAs representative of the MBL. The parameter, A_{tot}, was calculated for each aerosol mode and then A_{tot} for each of the modes summed to achieve the total RASA for each air mass. A summary of the calculated RASA values with details of the campaign dates and locations are shown in Table 6.

The RASA calculations established a range of values which were included in the detailed model. The lowest relevant value was $5.6\times10^{-8}\,cm^{-1}$, measured during the Aerosols99 campaign in the Northern Hemispheric Atlantic Ocean, (Bates et al., 2001). The highest relevant value of RASA was $4.2\times10^{-7}\,cm^{-1}$, the background marine value calculated from ship-based measurements near Tasmania (Bates et al., 1998). The larger sea-salt mode dominated as expected in remote MBL conditions. The average RASA value obtained was $2.73\times10^{-7}\,cm^{-1}$, significantly higher than the value of $1.0\times10^{-7}\,cm^{-1}$ quoted by Whitby and Sverdrup (1980).

The accommodation coefficients for OH and HO_2 in our model are parameterised as temperature dependent accommodation coefficients (Gratpanche et al., 1996) in Table 3, with no account taken of the surface characteristics. There are a few papers reporting uptake coefficients for both OH and HO_2 with lower limits quoted for the HO_2 coefficients due to experimental limitations, giving rise to a low confidence in current experimental values for HO_2 (Cooper and Abbatt, 1996; Hanson et al., 1992). The impact of reactions on aerosol on HO_2 concentrations in the remote atmosphere could be significant if the uptake coefficient was greater than 0.1, and could dominate if it was close to unity (Saylor, 1997).

When considering the impact of uptake by aerosol, the chemical composition of the aerosol is also likely to be significant. Bates et al. (1998, 2001) measured strong variations in the chemical composition of the Aitken, accommodation and sea-salt dominated coarse modes that would influence the free radical uptake rates, particularly the extent of aerosol acidification. Without data on the size segregated aerosol chemical composition during SOAPEX-2 and the relevant laboratory data, it is not possible to calculate accurate accommodation coefficients.

Table 6. Calculated values of RASA.

Campaign/location/dates	Air mass	RASA (cm^{-1})
Aerosols99, Atlantic Ocean, 14 Jan. to 8 Feb. 1999 [(a)]	NH marine 31° N to 15.5° N	5.6×10^{-8}
Aerosols99, Atlantic Ocean, 14 Jan. to 8 Feb. 1999 [(a)]	SH marine temperate 24.5° S to 33° S	1.8×10^{-7}
ACE1, Cape Grim, Tasmania, Nov.–Dec. 1995 [(b)]	Baseline sector 40.7° S, 144.7° E	2.0×10^{-7}
Punta Del Hidalgo, Tenerife, Canary Islands, July 1994 [(c)]	MBL-III Clean 28°18′ N, 16°30′ W	3.7×10^{-7}
Punta Del Hidalgo, Tenerife, Canary Islands, July 1994 [(c)]	MBL-IV Clean 28°18′ N, 16°30′ W	3.3×10^{-7}
ACE1-NOAA ship "Discoverer" Southern Ocean near Tasmania, Nov.–Dec. 1995 [(d)]	Background marine	4.2×10^{-7}

[(a)] Bates et al. (2001) mode fit parameters are for the number size distribution at 55% RH from measurements taken during the Aerosols99 campaign over the Atlantic Ocean.
[(b)] Covert et al. (1998) quote number of aerosol particles as cloud condensation nuclei (CCN) therefore underestimated when assumed equal to N_{tot}. Values for D were estimated from the number-size distribution.
[(c)] Raes et al. (1997).
[(d)] Bates et al. (1998) values for N_{tot} and D are quoted at 10% RH.

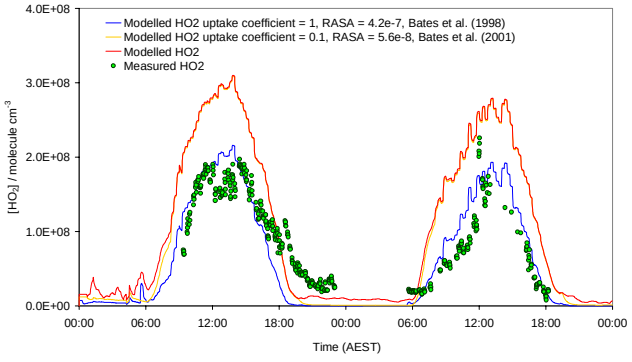

Fig. 8. Effect on $[HO_2]$ of changing uptake coefficient and RASA (15–16 February).

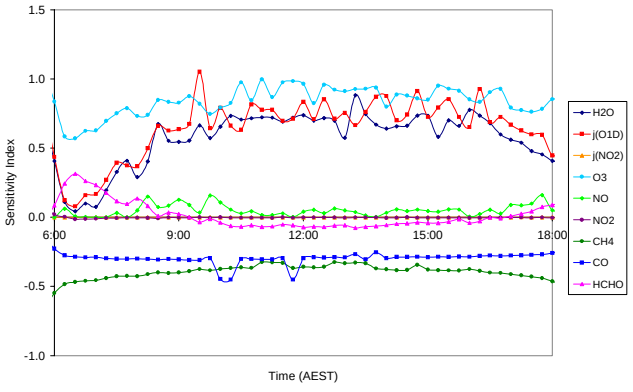

Fig. 9. Local Sensitivity Analysis of OH between 06:00 and 18:00 (7 February).

The model was run with the RASA at $5.6\times10^{-8}\,cm^{-1}$ and $4.2\times10^{-7}\,cm^{-1}$. The reaction probability for HO_2 was set to values of γ=0.1 and 1. The effect on concentrations of HO_2 is shown in Fig. 8. It is clear that, except during the night, the modelled concentrations are much closer to the measurements when the uptake rate was set to a higher value, i.e. with an accommodation coefficient equal to unity and a surface area of $4.2\times10^{-7}\,cm^{-1}$. This emphasises the need for accurate measurements of the RASA (including chemical composition) during a campaign and better measurements of accommodation coefficients in the laboratory.

Changing the HO_2 uptake coefficient and the RASA had little effect on [OH], because the recycling of OH from HO_2 is not very efficient in these low NO_x conditions as was shown in detail in Sect. 5.3. Also, the OH uptake coefficient and lifetime are small in comparison to those for HO_2 radicals.

5.5 Uncertainty analysis

Sensitivity analysis allows the study of the relationship between the input parameters and the output values of a model (Turanyi, 1990), whereas uncertainty analysis estimates output uncertainties from input uncertainties (Saltelli et al., 2000). In order to reduce complexity, the "simple" model was used for the sensitivity and the uncertainty analyses since

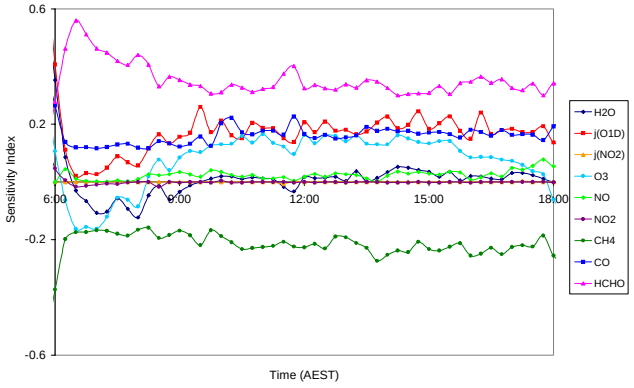

Fig. 10. Local Sensitivity Analysis of HO_2 between 06:00 and 18:00 (7 February).

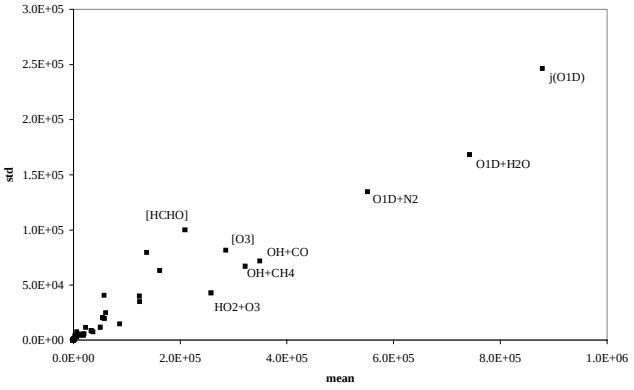

Fig. 11. Morris One-At-a-Time Analysis of OH for 7 February. Only the most significant parameters are indicated (std is standard deviation).

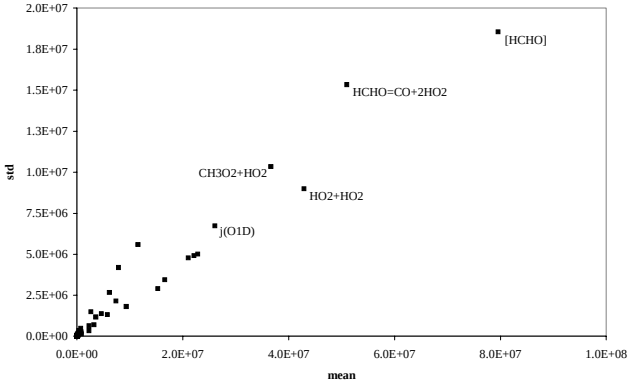

Fig. 12. Morris One-At-a-Time Analysis of HO_2 for 7 February Only the most significant parameters are indicated (std is standard deviation).

it includes only 92 reactions, yet provides comparable results to the more detailed model.

A brute force local sensitivity analysis was performed by changing the measured concentrations of H_2O, O_3, NO, NO_2, CH_4, CO, HCHO and the values of $j(O^1D)$ and $j(NO_2)$ by $\pm 1\%$ and examining the variation in the [OH] and $[HO_2]$ concentrations. The local sensitivity index (SI) was calculated as:

$$SI = \frac{\%\Delta X^{+1\%} - \%\Delta X^{-1\%}}{100 \times 0.02}, \quad (16)$$

where $\%\Delta X^{\pm 1\%}$ is the percentage variation in the concentration of species X when the input parameter is changed by $\pm 1\%$. The results for 7 February are shown in Figs. 9 and 10 for the period 06:00–18:00. The results are in accord with the rate of production analysis. [OH] shows a positive sensitivity to $[H_2O]$, $j(O^1D)$ and $[O_3]$, which directly influence OH formation and a negative sensitivity to the concentrations of species primarily responsible for its removal, CO and CH_4. [HCHO] shows the largest positive sensitivity for $[HO_2]$, because it acts as a photolysis source. $j(O^1D)$, [CO] and $[O_3]$ also have positive sensitivity indices, because of their influence on the rate of formation of OH or on its conversion to HO_2. $[CH_4]$, on the other hand, shows a negative sensitivity, because it reacts with OH to form CH_3O_2, which has a low probability of forming HO_2 in low NO_x conditions.

The OH sensitivity to HCHO is positive during the early morning-late afternoon and negative in the central part of the day. This is due to the relative importance of HCHO as OH sink and radical source. In the early morning OH+HCHO is comparable to OH+CH_3OOH and less than OH+H_2 (at 10:00 fluxes are: 1.6, 1.7 and 2.4×10^5 molecule cm^{-3} s^{-1}, respectively), but in the middle of the day OH+HCHO becomes more important than OH+CH_3OOH and as important as OH+H_2 (at 14:00 fluxes are: 4.0, 3.4 and 3.8×10^5 molecule cm^{-3} s^{-1}, respectively). On the other hand j(HCHO) is broader than $j(O^1D)$: in the early morning production of HO_2 by this route becomes the major radical production reaction. In addition since ozone photolysis is slow, HO_2+O_3 is a significant source of OH. So in the early morning late afternoon perturbing HCHO affects OH production from HCHO through HO_2 more than OH loss, thus giving a positive SI.

Local sensitivity analysis is of limited value when the chemical system is non-linear. In this case global methods, which vary the parameters over the range of their possible values, are preferable. Two global uncertainty methods have been used in this work, a screening method, the so-called Morris One-At-A-Time (MOAT) analysis and a Monte Carlo analysis with Latin Hypercube Sampling (Saltelli et al., 2000; Zádor et al., submitted, 2004[1]). The analyses were performed by varying rate parameters, branching ratios and constrained concentrations within their uncertainty interval,

[1] Zádor, J., Pilling, M. J., Wagner, V., and Wirtz, K.: Quantitative assessment of uncertainties for a model of tropospheric ethene oxidation using the European Photochemical Reactor, Atmos. Environ., submitted, 2004.

Table 7. Chemical mechanism used in the "simple model". Notation is in FACSIMILE format (see http://mcm.leeds.ac.uk/MCM/).

Rate Coefficient	Inorganic Mechanism
6.00D-34*O2*O2*((TEMP/300)@−2.6)+5.60D-34*O_2*N_2*((TEMP/300)@−2.6)	O=O_3
8.00D-12*EXP(−2060/TEMP)	O+O_3=
KMT01	O+NO=NO_2
5.50D-12*EXP(188/TEMP)	O+NO_2=NO
KMT02	O+NO_2=NO_3
3.20D-11*O_2*EXP(67/TEMP)+2.10D-11*N_2*EXP(115/TEMP)	O^1D=O
1.40D-12*EXP(−1310/TEMP)	NO+O_3=NO_2
1.40D-13*EXP(−2470/TEMP)	NO_2+O_3=NO_3
3.30D-39*EXP(530/TEMP)*O_2	NO+NO=NO_2+NO_2
1.80D-11*EXP(110/TEMP)	NO+NO_3=NO_2+NO_2
4.50D-14*EXP(−1260/TEMP)	NO_2+NO_3=NO+NO_2
KMT03 % KMT04	NO_2+NO_3=N_2O_5
2.20D-10*H_2O	O^1D=OH+OH
1.70D-12*EXP(−940/TEMP)	OH+O_3=HO_2
7.70D-12*EXP(−2100/TEMP)	OH+H_2=HO_2
1.30D-13*KMT05	OH+CO=HO_2
2.90D-12*EXP(−160/TEMP)	OH+H_2O_2=HO_2
2.03D-16*((TEMP/300)4.57)*EXP(693/TEMP)	HO_2+O_3=OH
4.80D-11*EXP(250/TEMP)	OH+HO_2=
2.20D-13*KMT06*EXP(600/TEMP)+1.90D-33*M*KMT06*EXP(980/TEMP)	HO_2+HO_2=H_2O_2
KMT07	OH+NO=HONO
KMT08	OH+NO_2=HNO_3
2.0D-11	OH+NO_3=HO_2+NO_2
3.60D-12*EXP(270/TEMP)	HO_2+NO=OH+NO_2
KMT09 & KMT10	HO_2+NO_2=HO_2NO_2
1.90D-12*EXP(270/TEMP)	OH+HO_2NO_2=NO_2
4.0D-12	HO_2+NO_3=OH+NO_2
2.50D-12*EXP(260/TEMP)	OH+HONO=NO_2
KMT11	OH+HNO_3=NO_3
1.8E-12*EXP(−240/TEMP)	OH+HCl=Cl
4.00D-32*EXP(−1000/TEMP)*M	O+SO_2=SO_3
KMT12	OH+SO_2=HSO_3
1.30D-12*EXP(−330/TEMP)*O_2	HSO_3=HO_2+SO_3
2.26D-43*TEMP*EXP(6544/TEMP)*H_2O*H_2O	SO_3=SA
1.0D-18	SO_2+HO_2=SO_3+OH
5.0D-17	SO_2+CH_3O_2=CH_3O+SO_3
2.50E-22	N_2O_5+H_2O=HNO_3+HNO_3
1.80E-39	N_2O_5+H_2O+H_2O=HNO_3+HNO_3+H_2O
8.5E-13*EXP(−2450/TEMP)	NO_3+NO_3=NO_2+NO_2
J1	O_3=O^1D
J2	O_3=O
J3	H_2O_2=OH+OH
J4	NO_2=NO+O
J5	NO_3= NO
J6	NO_3=NO_2+O
J7	HONO=OH+NO
J8	HNO_3=OH+NO_2

which were taken from the IUPAC (Atkinson et al., 2001) and JPL evaluations (DeMore et al., 1994) for the kinetic parameters and from the instrumental precision for the measured values.

The MOAT method (Saltelli et al., 2000; Zádor et al., submitted, 2004[2]) determines the effect of variations of

[2]Zádor, J., Pilling, M. J., Wagner, V., and Wirtz, K.: Quantitative assessment of uncertainties for a model of tropospheric ethene

Table 7. Continued.

Rate Coefficient	**Organic Mechanism**
9.65D-20*TEMP@2.58*EXP(−1082/TEMP)	$OH+CH_4=CH_3O_2$
9.60D-12*EXP(−1350/TEMP)	$Cl+CH_4=CH_3O_2$
1.00E-18	$NO_3+CH_4=CH_3O_2+HNO_3$
3.00D-12*EXP(280/TEMP)*0.999	$CH_3O_2+NO=CH_3O+NO_2$
3.00D-12*EXP(280/TEMP)*0.001	$CH_3O_2+NO=CH_3NO_3$
KMT13 % KMT14	$CH_3O_2+NO_2=CH_3O_2NO_2$
$KRO2NO_3$*0.40	$CH_3O_2+NO_3=CH_3O+NO_2$
3.80D-13*EXP(780/TEMP)	$CH_3O_2+HO_2=CH_3OOH$
1.82D-13*EXP(416/TEMP)*0.33*RO_2	$CH_3O_2=CH_3O$
1.82D-13*EXP(416/TEMP)*0.335*RO_2	$CH_3O_2=HCHO$
1.82D-13*EXP(416/TEMP)*0.335*RO_2	$CH_3O_2=CH_3OH$
7.20D-14*EXP(−1080/TEMP)*O_2	$CH_3O=HCHO+HO_2$
1.00D-14*EXP(1060/TEMP)	$OH+CH_3NO_3=HCHO+NO_2$
J51	$CH_3NO_3=CH_3O+NO_2$
1.90D-12*EXP(190/TEMP)	$OH+CH_3OOH=CH_3O_2$
1.00D-12*EXP(190/TEMP)	$OH+CH_3OOH=HCHO+OH$
J41	$CH_3OOH=CH_3O+OH$
1.20D-14*TEMP*EXP(287/TEMP)	$OH+HCHO=HO_2+CO$
J11	$HCHO=CO+HO_2+HO_2$
J12	$HCHO=H_2+CO$
5.80D-16	$NO_3+HCHO=HNO_3+CO+HO_2$
6.01D-18*TEMP@2*EXP(170/TEMP)	$CH_3OH+OH=HO_2+HCHO$
Rate Coefficient	**Heterogeneous Losses**
350.0*AREA*(TEMP@0.5)*GN_2O_5	$N_2O_5=$
633.24*AREA*(TEMP@0.5)*GHO_2	$HO_2=$
530.59*AREA*(TEMP@0.5)*GCH_3O_2	$CH_3O_2=$
882.23*AREA*(TEMP@0.5)*GOH	$OH=$
458.28*AREA*(TEMP@0.5)*$GHNO_3$	$HNO_3=$
461.97*AREA*(TEMP@0.5)*GNO_3	$NO_3=$
454.81*AREA*(TEMP@0.5)*GSO_2	$SO_2=$
623.99*AREA*(TEMP@0.5)*GH_2O_2	$H_2O_2=$
643.19*AREA*(TEMP@0.5)*GCH_3OH	$CH_3OH=$
Rate Coefficient	**Dry Deposition Processes**
(2.000)/HMIX	$HNO_3=$
(0.150)/HMIX	$NO_2=$
(0.500)/HMIX	$SO_2=$
(1.100)/HMIX	$H_2O_2=$
(0.550)/HMIX	$CH_3OOH=$
(0.500)/HMIX	$O_3=$
(0.330)/HMIX	$HCHO=$
(1.100)/HMIX	$CH_3NO_3=$

individual parameters (e.g. rate coefficients, branching ratios and measured concentrations) on [OH] and [HO_2]. Parameter sets are generated according to the Morris algorithm and the effect of a parameter is calculated from model runs with different values of the given parameter. From numerous model runs the mean and the standard deviation of the effect of a parameter is calculated. The mean shows the importance of the parameter, while the standard deviation shows the magnitude of the nonlinearity the parameter change implies. The mean effect of each parameter was plotted versus the standard deviation and the plots of 7 February for OH and HO_2 are shown in Figs. 11 and 12.

The Morris analysis confirms the results of the sensitivity analysis, while the clustering of the points around a single

oxidation using the European Photochemical Reactor, Atmos. Environ., submitted, 2004.

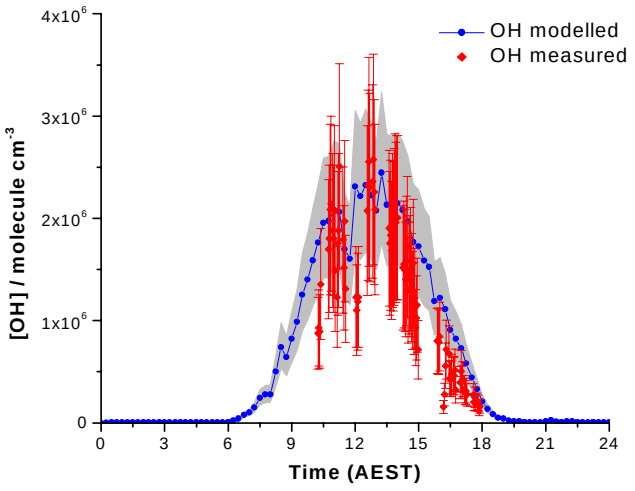

Fig. 13. Model-measurement comparison of OH with 2σ error bars (7 February).

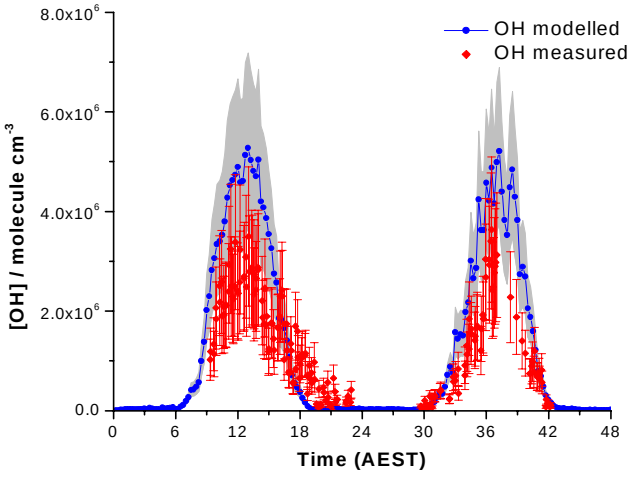

Fig. 14. Model-measurement comparison of OH with 2σ error bars (15–16 February).

curve suggests that non-linear and/or interactive effects are not substantial. For OH, the Morris analysis clearly identifies the importance of OH generation from ozone photolysis and illustrates the importance of reliable $j(O^1D)$ measurements and of the rate coefficients that determine the efficiency of the $O^1D \rightarrow OH$ conversion. The HO_2 analysis emphasizes the importance of reliable [HCHO] measurements, of the H atom production channel in HCHO photolysis and of the peroxy-peroxy radical chain termination reactions.

Quantum yields for formaldehyde photolysis have not received the same attention as those for ozone photolysis and are clearly important even in an unpolluted environment. The absorption spectrum is highly structured and more detailed measurements, under atmospheric conditions, are needed. In this work the uncertainty in HCHO measurements was estimated to be ~50%, which is probably a conservative estimate.

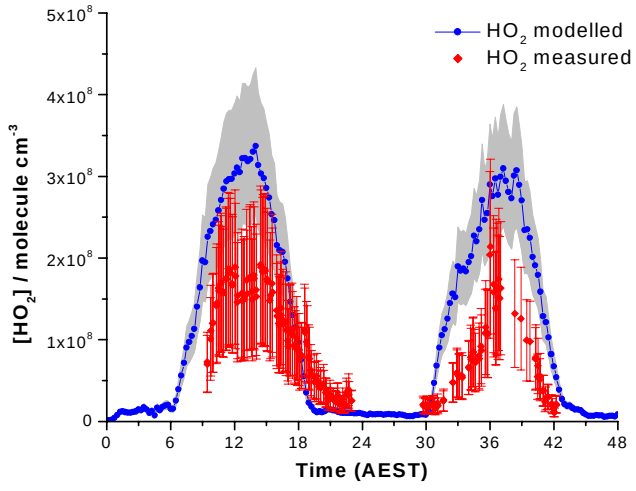

Fig. 15. Model-measurement comparison of HO_2 with 2σ error bars (15–16 February).

The box-models are not expected to correctly calculate the concentration of HCHO, but, given the importance of HCHO as shown by the Morris Analysis, it is interesting to see the effect of not constraining the models to HCHO measurements on $[HO_x]$. The "simple" model underestimates [HCHO] by about a factor of two, but because the main source of HO_2 is OH and the recycling from HO_2 to OH is slow under these conditions (Sect. 5.3), this reduces $[HO_2]$ by 15–25%. The effect is smaller for [OH] concentration (5–7%).

While the Morris analysis is computationally cheap and fast, it is only a screening method, providing qualitative information. The overall model uncertainty was determined by a Monte Carlo method, coupled with the Latin Hypercube Sampling (LHS) technique (Saltelli et al., 2000; Zádor et al., submitted, 2004[3]). A lognormal distribution was assumed for the rate coefficients, a uniform distribution for the branching ratios and a normal distribution for the input parameters (H_2O, O_3, NO, NO_2, CH_4, CO, HCHO, $j(O^1D)$, $j(NO_2)$, temperature). The means and the variances of the Monte Carlo simulation outputs were calculated from 500 Monte Carlo runs: assuming a lognormal distribution for the outputs, the 2σ standard deviation of the model was estimated to be 30–40% for OH and 25–30% for HO_2. The measurement uncertainties were 40% for OH and 50% for HO_2 (Creasey et al., 2003). The results are shown in Fig. 13 for 7 February (OH) and in Figs. 14 and 15 for 15–16 February (OH and HO_2).

[3]Zádor, J., Pilling, M. J., Wagner, V., and Wirtz, K.: Quantitative assessment of uncertainties for a model of tropospheric ethene oxidation using the European Photochemical Reactor, Atmos. Environ., submitted, 2004.

Figures 13, 14 and 15 show that the uncertainty ranges for model and measurement overlap for OH except in the evening of 15 February (Fig. 14), where, as noted earlier, the measured OH persists into the evening. The significance of the consistent overestimation by the model does need further investigation, however, despite the uncertainty overlap. A measure of the statistical significance of the overestimation would be of value. The comparison for HO_2 (Fig. 15) is much less satisfactory and there is little uncertainty overlap at any stage on 16 February, although the agreement on 15 February is better, except in the evening. The Morris analysis suggests that this overestimation may be related to HCHO, but that would require an uncertainty in the measured [HCHO] significantly greater than the estimated value of 50%. A more likely source of the discrepancy is an underestimation in the model of heterogeneous uptake of HO_2, as discussed above.

Data from a recent campaign (NAMBLEX) in Mace Head, Ireland, suggest that in the MBL halogen oxides, such as IO and BrO, may have a significant impact upon [HO_2]. IO was measured during one of the days investigated, 15 February, by DOAS (Table 1) with a maximum concentration of 0.8 ppt. The "simple" model was run with a basic IO mechanism (IO+HO_2, HOI photolysis, HOI heterogeneous loss) using estimated photolysis rates and simple heterogeneous uptake of HOI ($k=\frac{A\bar{c}\gamma}{4}$ with γ=0.6). The effect is that OH increases by ∼10% and HO_2 decreases by ∼10%. A proper calculation of the impact of halogen oxides on the [HO_x] in the MBL requires accurate photolysis rates and aerosol uptake rates. This rough calculation shows that the effect of IO is not negligible and is being considered in more detail in the NAMBLEX campaign (where [IO] was generally higher).

6 Summary and conclusions

Two observationally constrained box-models, based on the Master Chemical Mechanism and with different levels of chemical complexity, have been used to study the HO_x radical chemistry during the SOAPEX-2 campaign, which took place during the austral summer of 1999 (January–February) at the Cape Grim Baseline Air Pollution Station in northwestern Tasmania, Australia. The box-models were constrained to the measured values of long lived species and photolysis rates and physical parameters (NO, NO_2, O_3, HCHO, j(O^1D), j(NO_2), H_2O and temperature). In addition the "detailed" model was constrained to the measured concentration of CO, CH_4 and 17 NMHCs, while the "simple" model was additionally constrained only to CO and CH_4. The models were updated to the latest available kinetic data and completed with a simple description of the heterogeneous uptake and dry deposition processes.

The models were used to calculate [OH] and [HO_2] and the results were compared with the measurements performed by the FAGE instrument. Four days (7, 8, 15, and 16 February) were selected as representative of the extremely clean conditions of the Southern Hemisphere Marine Boundary Layer. These very clean conditions (NO<3 ppt) correspond to the cleanest conditions under which radical measurements have been taken at ground level in the Southern Pacific Ocean. The two models agree to within 5–10% or less.

The agreement between modelled and measured OH is within 10% on 7 and 8 February and 20% on 15 and 16 February around midday. Less satisfactory agreement was obtained for HO_2, using a simple heterogeneous uptake treatment, as the models overestimate it by about 40% on 15 and 16 February. By increasing the uptake coefficients (γ) for OH and HO_2 from 0.1 and 1 and increasing the reactive aerosol surface area (RASA) to 4.2×10^{-7} and 5.6×10^{-8} cm^{-1}, a better agreement with HO_2 measurements resulted, with little effect on OH, due to the low NO_x conditions of Cape Grim on these days.

A rate of production analysis shows that radical production occurs primarily via $O(^1D)+H_2O$, but with a significant contribution to HO_2 from HCHO photolysis. OH reacts mainly with CO and CH_4, followed by HCHO, H_2, O_3 and CH_3OOH with minor contributions from NMHCs. At the low NO concentrations encountered on these clean days, radical-radical reactions dominate the loss of peroxy-radicals resulting in a reduced chain propagation via CH_3O_2+NO and HO_2+NO and in a very short chain length (∼0.14), calculated as the rate of $HO_2\rightarrow$OH conversion divided by the total radical production rate.

The rate of production analysis was complemented by a local sensitivity analysis and by a global Morris screening analysis. These analyses demonstrate the necessity of accurate measurements of j(O^1D) and [HCHO] and reduced uncertainty in the quantum yields for H from HCHO photolysis.

Finally, a Monte Carlo method coupled with the Latin Hypercube Sampling (LHS) was used to assess the overall model uncertainty. The 2σ standard deviation of the model was estimated to be 30–40% for OH and 25–30% for HO_2, which is comparable to the instrumental uncertainty.

Acknowledgements. We gratefully acknowledge the support and the help of the (now) Commonwealth Bureau of Meteorology, of the CSIRO Melbourne and of the Cape Grim staff for during the SOAPEX-2 campaign, particularly L. Porter and J. Britton. We are also grateful to the staff of CSIRO Atmospheric Research. Thanks to G. Evans for technical assistance with the operation of the FAGE instrument during SOAPEX-2 and to the Universities of Leicester and East Anglia for the use of their data. A.-L. Haggerstone acknowledges the University of York for a PhD scholarship. R. Sommariva, J. Zádor and D. J. Creasey acknowledge the University of Leeds for scholarships. D. E. Heard would like to thank The Royal Society for a University Research Fellowship and some equipment funding. Financial support for this project was provided by the NERC, grant GR3/1A447.

Edited by: B. Sturges

References

Allan, B. J., Carslaw, N., Coe, H., Burgess, R. A., and Plane, J. M. C.: Observations of the nitrate radical in the Marine Boundary Layer, J. Atmos. Chem., 33, 129–154, 1999.

Allan, B. J., Plane, J. M. C., and McFiggans, G.: Observations of OIO in the remote marine boundary layer, Geophys. Res. Lett., 28, 1945–1948, 2001.

Atkinson, R., Baulch, D. L., Cox, R. A., Crowley, J. N., Hampson Jr., R. F., Kerr, J. A., Rossi, M. J., and Troe, J.: Summary of Evaluated Kinetic and Photochemical Data for Atmospheric Chemistry, IUPAC Subcommittee on Gas Kinetic Data Evaluation for Atmospheric Chemistry, http://www.iupac-kinetic.ch.cam.ac.uk, December 2001.

Ayers, G. P. and Galbally, I.: A preliminary investigation of a boundary layer – free troposphere entrainment velocity at Cape Grim, Baseline 92, Department of Arts, Sport, Environment, Tourism and Territories, Canberra A.C.T., Australia, 1994.

Ayers, G. P., Gillett, R. W., Granek, H., de Serves, C., and Cox, R. A.: Formaldehyde production in clean marine air, Geophys. Res. Lett., 24, 401–404, 1997.

Bates, T. S., Kapustin, V. N., Quinn, P. K., Covert, D. S., Coffman, D. J., Mari, C., Durkee, P. A., Bruyn, W. J. D., and Saltzman, E. S.: Processes controlling the distribution of aerosol particles in the lower marine boundary layer during the First Aerosol Characterization Experiment (ACE 1), J. Geophys. Res.-A., 103, 16 369–16 383, 1998.

Bates, T. S., Quinn, P. K., Coffman, D. J., Johnson, J. E., Miller, T. L., Covert, D. S., Wiedensohler, A., Leinert, S., Nowak, A., and Neususs, C.: Regional physical and chemical properties of the marine boundary layer aerosol across the Atlantic during Aerosols99: An overview, J. Geophys. Res.-A., 106, 20 767–20 782, 2001.

Bauguitte, S.: Rep. ENV4-CT95-0038, Geophys. Inst., University of Bergen, Bergen, Norway, 21–26, 1998.

Bauguitte, S.: Ph.D. Thesis, University of East Anglia, Norwich, UK, 2000.

Behnke, W., George, C., Scheer, V., and Zetzsch, C.: Production and decay of $ClNO_2$, from the reaction of gaseous N_2O_5 with NaCl solution: Bulk and aerosol experiments, J. Geophys. Res.-A., 102, 3795–3804, 1997.

Beichert, P. and Pitts, B. J. F.: Knudsen cell studies of the uptake of gaseous HNO_3 and other oxides of nitrogen on solid NaCl: The role of surface-adsorbed water, J. Phys. Chem., 100, 15 218–15 228, 1996.

Brasseur, G. P., Hauglustaine, D. A., Walters, S., Rasch, P. J., Muller, J. F., Granier, C., and Tie, X. X.: MOZART, a global chemical transport model for ozone and related chemical tracers 1.: Model description, J. Geophys. Res.-A., 103, 28 265–28 289, 1998.

Brauers, T., Hausmann, M., Bister, A., Kraus, A., and Dorn, H. P.: OH radicals in the boundary layer of the Atlantic Ocean 1.: Measurements by long-path laser absorption spectroscopy, J. Geophys. Res.-A., 106, 7399–7414, 2001.

Carpenter, L. J., Sturges, W. T., Penkett, S. A., Liss, P. S., Alicke, B., Hebestreit, K., and Platt, U.: Short-lived alkyl iodides and bromides at Mace Head, Ireland: Links to biogenic sources and halogen oxide production, J. Geophys. Res.-A., 104, 1679–1689, 1999.

Carpenter, L. J., Liss, P. S., and Penkett, S. A.: Marine organohalogens in the atmosphere over the Atlantic and Southern Oceans, J. Geophys. Res.-A., 108, doi:10.1029/2002JD002769, 2003.

Carslaw, N., Creasey, D. J., Heard, D. E., Lewis, A. C., McQuaid, J. B., Pilling, M. J., Monks, P. S., Bandy, B. J., and Penkett, S. A.: Modeling OH, HO_2, and RO_2 radicals in the marine boundary layer – 1. Model construction and comparison with field measurements, J. Geophys. Res.-A., 104, 30 241–30 255, 1999.

Carslaw, N., Creasey, D. J., Harrison, D., Heard, D. E., Hunter, M. C., Jacobs, P. J., Jenkin, M. E., Lee, J. D., Lewis, A. C., Pilling, M. J., Saunders, S. M., and Seakins, P. W.: OH and HO_2 radical chemistry in a forested region of north-western Greece, Atmos. Environ., 35, 4725–4737, 2001.

Carslaw, N., Creasey, D. J., Heard, D. E., Jacobs, P. J., Lee, J. D., Lewis, A. C., McQuaid, J. B., Pilling, M. J., Bauguitte, S., Penkett, S. A., Monks, P. S., and Salisbury, G.: Eastern Atlantic Spring Experiment 1997 (EASE97) – 2. Comparisons of model concentrations of OH, HO_2, and RO_2 with measurements, J. Geophys. Res.-A., 107, doi:10.1029/2001JD001568, 2002.

Chen, G., Davis, D., Crawford, J., Heikes, B., O'Sullivan, D., Lee, M., Eisele, F., Mauldin, L., Tanner, D., Collins, J., Barrick, J., Anderson, B., Blake, D., Bradshaw, J., Sandholm, S., Carroll, M., Albercook, G., and Clarke, A.: An assessment of HO_x chemistry in the tropical Pacific boundary layer: Comparison of model simulations with observations recorded during PEM tropics A, J. Atmos. Chem., 38, 317–344, 2001.

Cooper, P. L. and Abbatt, J. P. D.: Heterogeneous interactions of OH and HO_2 radicals with surfaces characteristic of atmospheric particulate matter, J. Phys. Chem., 100, 2249–2254, 1996.

Covert, D. S., Gras, J. L., Wiedensohler, A., and Stratmann, F.: Comparison of directly measured CCN with CCN modeled from the number-size distribution in the marine boundary layer during ACE 1 at Cape Grim, Tasmania, J. Geophys. Res.-A., 103, 16 597–16 608, 1998.

Creasey, D. J., Heard, D. E., and Lee, J. D.: Eastern Atlantic Spring Experiment 1997 (EASE97) 1. Measurements of OH and HO_2 concentrations at Mace Head, Ireland, J. Geophys. Res.-A., 107, doi:10.1029/2001JD000892, 2002.

Creasey, D. J., Evans, G. E., Heard, D. E., and Lee, J. D.: Measurements of OH and HO_2 concentrations in the Southern Ocean marine boundary layer, J. Geophys. Res.-A., 108, doi:10.1029/2002JD003206, 2003.

Cunnold, D. M., Steele, L. P., Fraser, P. J., Simmonds, P. G., Prinn, R. G., Weiss, R. F., Porter, L. W., Langenfelds, R. L., Krummel, P. B., Wang, H. J., Emmons, L., Tie, X. X., and Dlugokencky, E. J.: In situ measurements of atmospheric methane at GAGE/AGAGE sites during 1985 to 1999 and resulting source inferences, J. Geophys. Res., 107, D14, doi:10.1029/2001JD001226, 2002.

Davis, D., Crawford, J., Liu, S., McKeen, S., Bandy, A., Thornton, D., Rowland, F., and Blake, D.: Potential impact of iodine on tropospheric levels of ozone and other critical oxidants, J. Geophys. Res.-A., 101, 2135–2147, 1996.

DeBruyn, W. J., Shorter, J. A., Davidovits, P., Worsnop, D. R., Zahniser, M. S., and Kolb, C. E.: Uptake of Gas-Phase Sulfur Species Methanesulfonic-Acid, Dimethylsulfoxide, and Dimethyl Sulfone by Aqueous Surfaces, J. Geophys. Res.-A., 99, 16 927–16 932, 1994.

DeMore, W. B., Sander, S., Golden, D., Hampson, R., Kurylo, M.,

Howard, C., Ravishankara, A., Kolb, C., and Molina, M.: Chemical Kinetics and Photochemical Data for Use in Stratospheric Modeling: Evaluation 11, Jet Propulsion Laboratory, Pasadena, California, USA, 1994.

Derwent, R. G., Jenkin, M. E., and Saunders, S. M.: Photochemical ozone creation potentials for a large number of reactive hydrocarbons under European conditions, Atmos. Environ., 30, 181–199, 1996.

Duan, S. X., Jayne, J. T., Davidovits, P., Worsnop, D. R., Zahniser, M. S., and Kolb, C. E.: Uptake of Gas-Phase Acetone by Water Surfaces, J. Phys. Chem., 97, 2284–2288, 1993.

Eisele, F. L., Tanner, D. J., Cantrell, C. A., and Calvert, J. G.: Measurements and steady state calculations of OH concentrations at Mauna Loa observatory, J. Geophys. Res.-A., 101, 14 665–14 679, 1996.

Finlayson-Pitts, B. J. and Pitts, J. N.: Chemistry of the upper and lower atmosphere, Academic Press, San Diego, California, USA, 2000.

Frost, G. J., Trainer, M., Mauldin, R. L., Eisele, F. L., Prevot, A. S. H., Flocke, S. J., Madronich, S., Kok, G., Schillawski, R. D., Baumgardner, D., and Bradshaw, J.: Photochemical modeling of OH levels during the first aerosol characterization experiment (ACE 1), J. Geophys. Res.-A., 104, 16 041–16 052, 1999.

George, L. A., Hard, T. M., and O'Brien, R. J.: Measurement of free radicals OH and HO_2 in Los Angeles smog, J. Geophys. Res.-A., 104, 11 643–11 655, 1999.

Gershenzon, Y. M., Grigorieva, V. M., Ivanov, A. V., and Remorov, R. G.: O_3 and OH sensitivity to heterogeneous sinks of HO_x and CH_3O_2 on aerosol particles, Faraday Discussions, 83–100, 1995.

Gras, J. L. and Ayers, G. P.: Marine Aerosol at Southern Mid-Latitudes, J. Geophys. Res.-O & A., 88, 661–666, 1983.

Gratpanche, F., Ivanov, A., Devolder, P., Gershenzon, Y., and Sawerysyn, J.-P.: Uptake coefficients of OH and HO_2 radicals on material surfaces of atmospheric interest, 14 International Symposium on Gas Kinetics, Leeds, September, 1996.

Grenfell, J. L., Savage, N. H., Harrison, R. M., Penkett, S. A., Forberich, O., Comes, F. J., Clemitshaw, K. C., Burgess, R. A., Cardenas, L. M., Davison, B., and McFadyen, G. G.: Tropospheric box-modelling and analytical studies of the hydroxyl (OH) radical and related species: Comparison with observations, J. Atmos. Chem., 33, 183–214, 1999.

Hanson, D. R., Burkholder, J. B., Howard, C. J., and Ravishankara, A. R.: Measurement of OH and HO_2 Radical Uptake Coefficients on Water and Sulfuric-Acid Surfaces, J. Phys. Chem., 96, 4979–4985, 1992.

Heard, D. E. and Pilling, M. J.: Measurement of OH and HO_2 in the troposphere, Chemical Reviews, 103, 12, 5163–5198, 2003.

Jayne, J. T., Duan, S. X., and Davidovits, P.: Uptake of gas-phase alcohol and organic acid molecules by water surfaces, J. Phys. Chem., 95, 6329–6336, 1991.

Jenkin, M. E., Clement, C., and Ford, I.: Gas-to-particle conversion pathways, First annual report on the contract: Met2a/1053/Project 2, AEA Technology, 1996.

Jenkin, M. E., Saunders, S. M., and Pilling, M. J.: The tropospheric degradation of volatile organic compounds: A protocol for mechanism development, Atmos. Environ., 31, 81–104, 1997.

Jenkin, M. E., Saunders, S. M., Wagner, V., and Pilling, M. J.: Protocol for the development of the Master Chemical Mechanism, MCM v3 (Part B): tropospheric degradation of aromatic volatile organic compounds, Atmos. Chem. Phys., 3, 181–193, 2003.

Kanaya, Y., Sadanaga, Y., Matsumoto, J., Sharma, U. K., Hirokawa, J., Kajii, Y., and Akimoto, H.: Daytime HO_2 concentrations at Oki Island, Japan, in summer 1998: Comparison between measurement and theory, J. Geophys. Res.-A., 105, 24 205–24 222, 2000.

Kanaya, Y., Matsumoto, J., Kato, S., and Akimoto, H.: Behavior of OH and HO_2 radicals during the Observations at a Remote Island of Okinawa (ORION99) field campaign 2.: Comparison between observations and calculations, J. Geophys. Res.-A., 106, 24 209–24 223, 2001.

Keene, W., Jacob, D. J., and Fan, S. M.: Reactive chlorine: A potential sink for dimethylsulfide and hydrocarbons in the marine boundary layer, Atmos. Environ., 30, R1–R3, 1996.

Koga, S. and Tanaka, H.: Numerical Study of the Oxidation Process of Dimethylsulfide in the Marine Atmosphere, J. Atmos. Chem., 17, 201–228, 1993.

Lewis, A. C., Carpenter, L. J., and Pilling, M. J.: Nonmethane hydrocarbons in Southern Ocean boundary layer air, J. Geophys. Res.-A., 106, 4987–4994, 2001.

McFiggans, G., Plane, J. M. C., Allan, B. J., Carpenter, L. J., Coe, H., and O'Dowd, C.: A modeling study of iodine chemistry in the Marine Boundary Layer, J. Geophys. Res., 105, 14 371–14 385, 2000.

Monks, P. S., Carpenter, L. J., Penkett, S. A., and Ayers, G. P.: Night-time peroxy radical chemistry in the remote marine boundary layer over the Southern ocean, Geophys. Res. Lett., 23, 535–538, 1996.

Monks, P. S., Carpenter, L. J., Penkett, S. A., Ayers, G. P., Gillett, R. W., Galbally, I. E., and Meyer, C. P.: Fundamental ozone photochemistry in the remote marine boundary layer: The SOAPEX experiment, measurement and theory, Atmos. Environ., 32, 3647–3664, 1998.

Penkett, S. A., Monks, P. S., Carpenter, L. J., Clemitshaw, K. C., Ayers, G. P., Gillett, R. W., Galbally, I. E., and Meyer, C. P.: Relationships between ozone photolysis rates and peroxy radical concentrations in clean marine air over the Southern Ocean, J. Geophys. Res.-A., 102, 12 805–12 817, 1997.

Prinn, R. G., Weiss, R. F., Fraser, P. J., Simmonds, P. G., Cunnold, D. M., Alyea, F. N., O'Doherty, S., Salameh, P., Miller, B. R., Huang, J., Wang, R. H. J., Hartley, D. E., Harth, C., Steele, L. P., Sturrock, G., Midgley, P. M., and McCulloch, A.: A history of chemically and radiatively important gases in air deduced from ALE/GAGE/AGAGE, J. Geophys. Res., 105, 17 751–17 792, 2000.

Pszenny, A. A. P., Keene, W. C., Jacob, D. J., Fan, S., Maben, J. R., Zetwo, M. P., Springeryoung, M., and Galloway, J. N.: Evidence of inorganic chlorine gases other than hydrogen-chloride in marine surface air, Geophys. Res. Lett., 20, 699–702, 1993.

Raes, F., VanDingenen, R., Cuevas, E., VanVelthoven, P. F. J., and Prospero, J.: Observations of aerosols in the free troposphere and marine boundary layer of the subtropical Northeast Atlantic: Discussion of processes determining their size distribution, J. Geophys. Res.-A., 102, 21 315–21 328, 1997.

Ravishankara, A. R.: Heterogeneous and multiphase chemistry in the troposphere, Science, 276, 1058–1065, 1997.

Ravishankara, A. R., Dunlea, E. J., Blitz, M. A., Dillon, T. J., Heard, D. E., Pilling, M. J., Strekowski, R. S., Nicovich, J. M., and Wine, P. H.: Redetermination of the rate coefficient for the re-

action of $O(^1D)$ with N_2, Geophys. Res. Lett., 29, art. no. 1745, 2002.

Rudich, Y., Talukdar, R. K., and Ravishankara, A. R.: Reactive uptake of NO_3 on pure water and ionic solutions, J. Geophys. Res.-A., 101, 21 023–21 031, 1996.

Saltelli, A., Chan, K., and Scott, E. M.: Sensitivity Analysis, Wiley & Sons Ltd., Chichester, 2000.

Sander, R.: Modeling atmospheric chemistry: Interactions between gas-phase species and liquid cloud/aerosol particles, Surv. Geophys., 20, 1–31, 1999.

Saunders, S. M., Jenkin, M. E., Derwent, R. G., and Pilling, M. J.: Protocol for the development of the Master Chemical Mechanism, MCMv3 (Part A): tropospheric degradation of non-aromatic volatile organic compounds, Atmos. Chem. Phys., 3, 161–180, 2003.

Saylor, R. D.: An estimate of the potential significance of heterogeneous loss to aerosols as an additional sink for hydroperoxy radicals in the troposphere, Atmos. Environ., 31, 3653–3658, 1997.

Stevens, P. S., Mather, J. H., Brune, W. H., Eisele, F., Tanner, D., Jefferson, A., Cantrell, C., Shetter, R., Sewall, S., Fried, A., Henry, B., Williams, E., Baumann, K., Goldan, P., and Kuster, W.: HO_2/OH and RO_2/HO_2 ratios during the Tropospheric OH Photochemistry Experiment: Measurement and theory, J. Geophys. Res.-A., 102, 6379–6391, 1997.

Tan, D., Faloona, I., Simpas, J. B., Brune, W., Olson, J., Crawford, J., Avery, M., Sachse, G., Vay, S., Sandholm, S., Guan, H. W., Vaughn, T., Mastromarino, J., Heikes, B., Snow, J., Podolske, J., and Singh, H.: OH and HO_2 in the tropical Pacific: Results from PEM-Tropics B, J. Geophys. Res.-A., 106, 32 667–32 681, 2001.

Turanyi, T.: Reduction of Large Reaction-Mechanisms, New J. Chem., 14, 795–803, 1990.

Whitby, K. T. and Sverdrup, G. M.: California aerosols: their physical and chemical characteristics, Adv. Environ. Sci. Technol., 9, 477–517, 1980.

Worsnop, D. R., Zahniser, M. S., Kolb, C. E., Gardner, J. A., Watson, L. R., Vandoren, J. M., Jayne, J. T., and Davidovits, P.: Temperature-Dependence of Mass Accommodation of SO_2 and H_2O_2 on Aqueous Surfaces, J. Phys. Chem., 93, 1159–1172, 1989.

Yin, F. D., Grosjean, D., Flagan, R. C., and Seinfeld, J. H.: Photooxidation of Dimethyl Sulfide and Dimethyl Disulfide – 2. Mechanism Evaluation, J. Atmos. Chem., 11, 365–399, 1990a.

Yin, F. D., Grosjean, D., and Seinfeld, J. H.: Photooxidation of Dimethyl Sulfide and Dimethyl Disulfide – 1. Mechanism Development, J. Atmos. Chem., 11, 309–364, 1990b.